Molecular Therapy
Original Article

Combined thioredoxin reductase and glutaminase inhibition exerts synergistic anti-tumor activity in MYC-high high-grade serous ovarian carcinoma

Prahlad V. Raninga,[1] Yaowu He,[2] Keshava K. Datta,[3] Xue Lu,[1] Uma R. Maheshwari,[1] Pooja Venkat,[4] Chelsea Mayoh,[4] Harsha Gowda,[1] Murugan Kalimutho,[1] John D. Hooper,[2] and Kum Kum Khanna[1]

[1]QIMR Berghofer Medical Research Institute, 300 Herston Road, Herston, Brisbane, QLD 4006, Australia; [2]Mater Research Institute, The University of Queensland, Translational Research Institute, Woolloongabba, QLD 4102, Australia; [3]Proteomics and Metabolomics Platform, La Trobe University, Melbourne, VIC 3086, Australia; [4]Children's Cancer Institute, Lowy Cancer Centre, UNSW Sydney, Kensington, NSW 2750, Australia

Approximately 50%–55% of high-grade serous ovarian carcinoma (HGSOC) patients have MYC oncogenic pathway activation. Because MYC is not directly targetable, we have analyzed molecular pathways enriched in MYC-high HGSOC tumors to identify potential therapeutic targets. Here, we report that MYC-high HGSOC tumors show enrichment in genes controlled by NRF2, an antioxidant signaling pathway, along with increased thioredoxin redox activity. Treatment of MYC-high HGSOC tumors cells with US Food and Drug Administration (FDA)-approved thioredoxin reductase 1 (TrxR1) inhibitor auranofin resulted in significant growth suppression and apoptosis in MYC-high HGSOC cells *in vitro* and also significantly reduced tumor growth in an MYC-high HGSOC patient-derived tumor xenograft. We found that auranofin treatment inhibited glycolysis in MYC-high cells via oxidation-induced GAPDH inhibition. Interestingly, in response to auranofin-induced glycolysis inhibition, MYC-high HGSOC cells switched to glutamine metabolism for survival. Depletion of glutamine with either glutamine starvation or glutaminase (GLS1) inhibitor CB-839 exerted synergistic anti-tumor activity with auranofin in HGSOC cells and OVCAR-8 cell line xenograft. These findings suggest that applying a combined therapy of GLS1 inhibitor and TrxR1 inhibitor could effectively treat MYC-high HGSOC patients.

INTRODUCTION

Epithelial ovarian cancer (OC) is the fifth most common cause of female cancer death worldwide and is the most lethal gynecological malignancy.[1] Most epithelial OCs are of the serous subtype. Furthermore, an overwhelming majority (90%) of serous ovarian carcinomas (SOCs) are high grade (HGSOC), contributing to high lethality for this subtype of OC.[2] Large-scale genomic data have demonstrated that HGSOC tumors are characterized by extensive copy number changes, and 50% of HGSOC patients have MYC amplification or pathway activation.[3] Despite the high incidence of MYC amplification in HGSOCs and in other solid tumors, MYC remains un-druggable because therapies targeting MYC have been unsuccessful in clinical trials. Hence an alternate therapeutic strategy is to identify MYC-regulated druggable signaling pathways, which can be inhibited using small molecule inhibitors.

MYC is a transcription factor that drives cancer progression by regulating genes involved in a plethora of biological processes, including metabolic processes such as glycolysis[4] and glutaminase metabolism,[5] and genes involved in maintaining intracellular redox homeostasis, such as NRF2-driven antioxidant pathways.[6] Increased intracellular oxidative stress is one of the hallmarks of cancer.[7,8] Although increased oxidative stress can be detrimental to cancer cells, MYC-active tumors survive such high oxidative stress as a result of increased NRF2-mediated antioxidant genes that protect tumor cells against increased oxidative stress. One of the key antioxidant systems transcriptionally regulated by NRF2 is the thioredoxin system. The expression of the components of the thioredoxin system, including thioredoxin and thioredoxin reductase 1 (TrxR1), is upregulated in multiple human cancers.[9–11] The thioredoxin system regulates the function of multiple signaling pathways involved in tumorigenesis by modulating the oxidation-reduction status. Pharmacological inhibition of TrxR1 using a gold-based anti-inflammatory drug US Food and Drug Administration (FDA) approved against rheumatoid arthritis, auranofin, has shown anti-cancer activity in multiple cancers.[9,10,12–14] Auranofin is currently in clinical trials for potential repurposing against cancer. However, cellular response to auranofin varies considerably; it is important to identify factors that influence anti-cancer effects of auranofin. Because MYC-high tumors cells have enrichment of NRF2 and its associated glycolysis gene signature, auranofin may represent an attractive drug candidate for MYC-high tumors.

Received 6 July 2022; accepted 15 December 2022;
https://doi.org/10.1016/j.ymthe.2022.12.011.

Correspondence: Prahlad V. Raninga, QIMR Berghofer Medical Research Institute, 300 Herston Road, Herston, Brisbane, QLD 4006, Australia.
E-mail: prahlad.raninga@qimrberghofer.edu.au
Correspondence: Kum Kum Khanna, QIMR Berghofer Medical Research Institute, 300 Herston Road, Herston, Queensland 4006, Australia.
E-mail: kumkum.khanna@qimrberghofer.edu.au

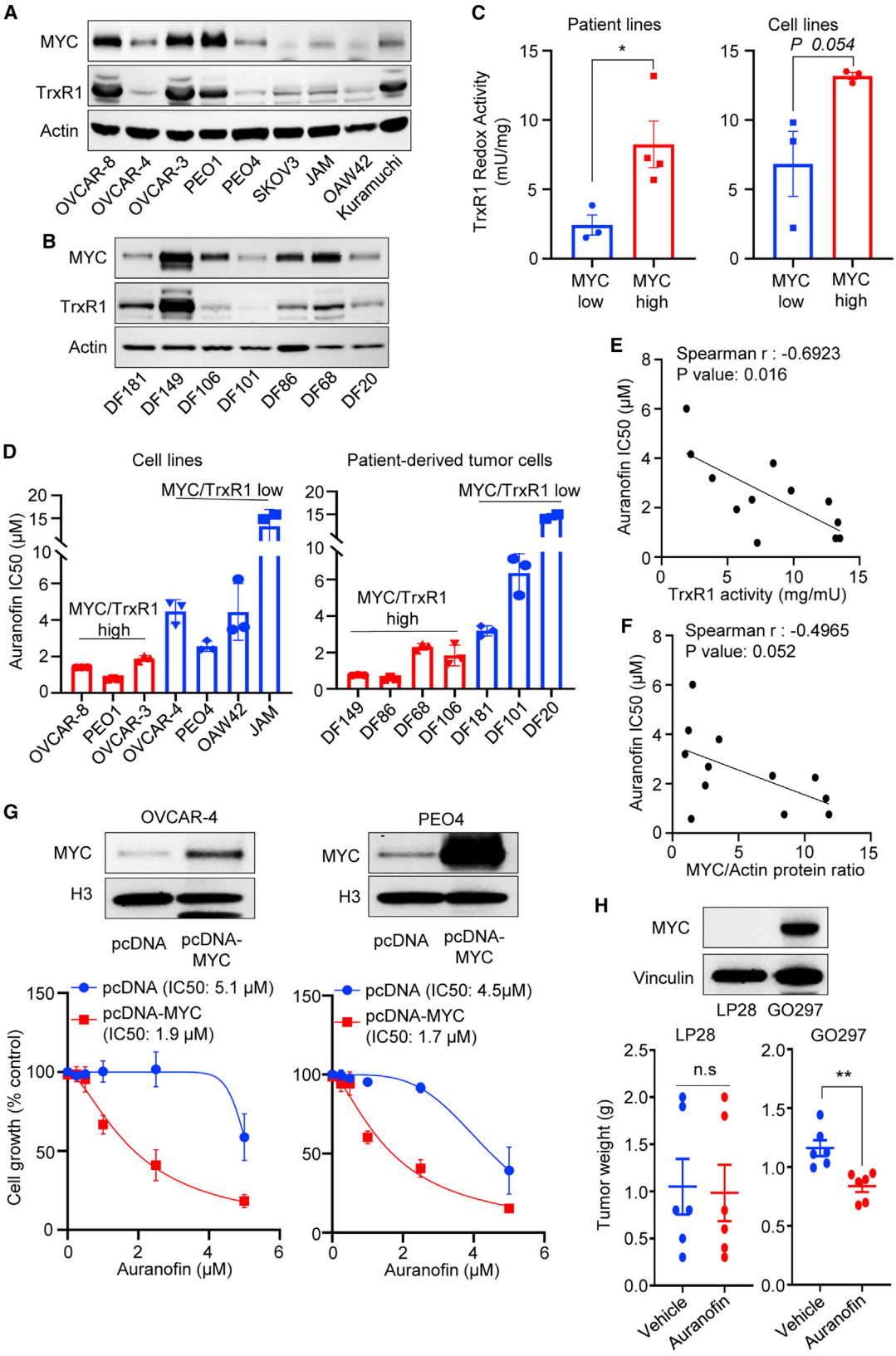

(legend on next page)

Glucose and glutamine are two major extracellular carbon sources responsible for fueling increased energy demand of tumor cells. On inhibition of one major cellular metabolic pathway, cancer cells often switch to an alternate metabolic pathway to fuel increased energy demand for survival.[15,16] Glutamine is the most abundant non-essential amino acid present in the blood plasma and also in proliferating cancer cells.[17] Once taken up by tumor cells, glutamine is converted into glutamate catalyzed by glutaminase 1 (GLS1) enzyme.[18] Glutamate and downstream metabolites feed into the tricarboxylic acid (TCA) cycle and generate macromolecules for nucleotide biosynthesis.[19,20] Multiple tumor types have shown dependency on the glutamine pathway via upregulation of GLS1. Pharmacological or genetic suppression of GLS1 exerts anti-tumor activity across a variety of cancers, including lymphoma, glioma, leukemia, triple-negative breast cancer, melanoma, non-small cell lung cancer, and renal cancer.[18,21–26] Several pharmacological inhibitors for GLS1 have been developed in recent years, including CB-839.[20,24] MYC upregulates transcription of glutamine pathway genes in OCs, and pharmacological inhibition of GLS1 using CB-839 exerted significant anti-tumor activity in OC models.[5] Because MYC regulates two major contributors to cellular metabolism, glycolysis and the glutamine pathway, co-inhibition of these two metabolic processes may be a promising therapeutic approach in MYC-high OCs.

In this study, we showed that MYC-high HGSOC tumors have enriched NRF2 gene signature and increased thioredoxin redox activity. Blocking thioredoxin activity through an FDA-approved inhibitor, auranofin, selectively suppressed the growth of MYC-high HGSOC cells via glycolysis inhibition, which in turn activates glutamine metabolism. Combined inhibition of glutamine metabolism using CB-839 with auranofin exerted synergistic anti-cancer activity in MYC-high HGSOCs.

RESULTS

Auranofin inhibits cell proliferation and induces apoptosis in MYC-high HGSOC cells

The MYC pathway is activated in 50%–55% of HGSOC tumors;[27,28] however, it remains undruggable to date because no specific drug is available to directly target MYC. An alternate strategy to target MYC-high tumor is to disrupt cellular pathways on which MYC-high tumors are dependent for survival.[29–31] To identify potentially targetable pathways, we first performed gene set enrichment analysis (GSEA) using Hallmarks gene sets and gene sets representing potential regulation by transcription factors in MYC-high and MYC-low OC patients using The Cancer Genome Atlas (TCGA). We found an enrichment of multiple gene signatures, including known MYC targets E2F-target genes, FOXM1-target genes, cell cycle, and cell proliferation (Table S1). Interestingly, we also found an enrichment of NRF2-driven gene signature in MYC-high HGSOC patients compared with MYC-low patients (Figure S1A). NRF2 is a master regulator of antioxidant genes and plays a crucial role in protecting tumor cells against elevated oxidative stress.[32] The thioredoxin system is one of the major cellular antioxidant systems and is transcriptionally regulated by NRF2.[33] We therefore initially analyzed the expression pattern of MYC and TrxR1 protein levels, as well as TrxR1 redox activity, in a panel of HGSOC cell lines (Figure 1A) and patient-derived HGSOC tumors cells (Figure 1B). Notably, high-MYC-expressing lines exhibited significantly higher basal reactive oxygen species (ROS) levels (Figure S1B). Interestingly, high MYC protein levels correlated with high TrxR1 protein levels (Figure S1C) and increased TrxR1 redox activity (Figure 1C) in cell lines and patient-derived HGSOC tumor cells. To further confirm whether MYC contributes to the regulation of TrxR1 expression in HGSOC cells, we depleted MYC expression in PEO1 cells using MYC-specific small interfering RNAs (siRNAs) and found that MYC knockdown markedly reduced TrxR1 protein levels in PEO1 cells (Figure S1D). Taken together, HGSOC tumors are dependent on the thioredoxin system to overcome MYC-induced oxidative stress.

We next examined the effect of TrxR1 inhibition on cell growth using an FDA-approved TrxR1 inhibitor, auranofin,[34] on a panel of established HGSOC cell lines and patient-derived HGSOC cells expressing varying levels of MYC protein (Figures 1A and 1B). MYC-high cell lines, including OVCAR-8 and PEO1, were most sensitive to auranofin (IC50 < 1 μM) compared with MYC-low cell lines (IC50 > 2.5 μM) (Figures 1D and S2A). Similarly, patient-derived tumor cells with high MYC protein levels, including DF149, DF86, DF106, and DF68, were most sensitive to auranofin (IC50 < 1 μM) compared with the MYC-low lines DF181, DF101, and DF20 (IC50 > 3.5 μM) (Figures 1D and S2A). Furthermore, our Spearman correlation analysis revealed that auranofin IC50 strongly correlates with TrxR1 redox activity (Figure 1E) and MYC protein levels (Figure 1F) in HGSOC cell lines and patient-derived tumor cells. Because TrxR1 is a selenoprotein, and cell culture media are often deficient in selenium,[35,36] we confirmed that auranofin inhibited the growth of MYC/TrxR1-high HGSOC cells at the similar IC50 concentrations (<1 μM) in media supplemented with selenium (Figure S2B). Additionally, we also observed that auranofin

Figure 1. Auranofin inhibits cell proliferation and induces apoptosis in MYC-high HGSOC cells

(A and B) MYC and TrxR1 protein levels were analyzed in a panel of established HGSOC cell lines (A) and patient-derived HGSOC tumor cells (B) using western blot. (C) Thioredoxin reductase 1 (TrxR1) redox activity was analyzed in MYC-low (blue) and MYC-high (red) patient-derived HGSOC tumor cells and in established HGSOC cell lines. Unpaired Student's t test, n = 3 (mean ± SEM). (D) The IC50 values of auranofin in each HGSOC cell line and patient-derived tumor cell line are shown. One-way ANOVA followed by Tukey's post-test, n = 3 (mean ± SEM). (E) Spearman correlation analysis between auranofin IC50 values and TrxR1 redox activity in established HGSOC cell lines and patient-derived tumor cells. (F) Spearman correlation analysis between auranofin IC50 values and MYC protein levels in established HGSOC cell lines and patient-derived tumor cells. (G) OVCAR-4 and PEO4 cells were transfected with either pcDNA vector (blue) or pcDNA-MYC plasmid (red) for 24 h. After 24-h transfection, cells were treated with auranofin (0–5 μM) for 6 days, and cell proliferation was analyzed. One-way ANOVA followed by Tukey's post-test, n = 3 (mean ± SEM). (H) LP28 (MYC-low) and GO297 (MYC-high) HGSOC PDX tumor growth following vehicle or auranofin administration (10 mg/kg, Monday–Friday, i.p.) after 2-week treatment. The weight of individual PDX tumors and their mean tumor size is presented. Unpaired Student's t test, n = 6 mice/group (mean ± SEM).

treatment (1 and 2.5 μM) resulted in PARP1 and caspase-3 cleavage, classical markers for apoptosis, in MYC-high lines (OVCAR-8, PEO1, and DF149), but not in MYC-low lines (OVCAR-4 and PEO4) (Figure S2C), suggesting that high-MYC expression sensitizes HGSOC cells to auranofin-induced cell death. Consistent with this, overexpression of MYC in MYC-low OVCAR-4 and PEO4 cells significantly increased TrxR1 redox activity (Figure S2D) and sensitized them to auranofin-induced growth inhibition (Figure 1G). The IC50 value of auranofin shifted from 5.1 μM in parental OVCAR-4 to 1.9 μM in MYC-overexpressing OVCAR-4 cells and from 4.5 μM in parental PEO4 cells to 1.7 μM in MYC-overexpressing PEO4 cells (Figure 1G). These data suggest that MYC-high HGSOC cells have strong survival dependency on TrxR1 activity compared with MYC-low HGSOCs, and hence MYC/TrxR1-high HGSOC cells have increased sensitivity to auranofin.

Auranofin has been shown to have other targets in addition to TrxR1 by which it induces apoptosis in cancer cells. To decipher whether auranofin exerts its growth-inhibitory effect in MYC/TrxR1-high HGSOC cells via TrxR1, we depleted TrxR1 expression using TrxR1-specific siRNAs in OVCAR-8 and PEO1 cells and compared anticancer activity of auranofin (0–2.5 μM) in control or TrxR1-depleted OVCAR-8 and PEO1 cells. Interestingly, TrxR1 depletion significantly rescued OVCAR-8 and PEO1 cells from auranofin-induced cell death, suggesting that auranofin exerts its anti-cancer effect via TrxR1 inhibition (Figure S3A). Furthermore, we also examined whether MYC/TrxR1-high HGSOC cells are more sensitive to a specific TrxR1 inhibitor, TRi-1,[37,38] compared with MYC/TrxR1-low HGSOC cells. MYC/TrxR1-high cell lines, including OVCAR-8, PEO1, and OVCAR-3, were more sensitive to TRi-1 (IC50 < 2.5–5 μM) compared with MYC-low cell lines (IC50 > 10 μM) (Figure S3B). Similar results were observed in cells growing in a media supplemented with selenium (Figure S3C).

Next, we tested *in vivo* anticancer activity of auranofin using an MYC-high (GO297) and MYC-low (LP28) HGSOC patient-derived tumor xenograft (PDX) by engrafting tumors cells into NRG mice followed by treatment with vehicle or auranofin after detection of palpable tumors, and we measured tumor nodules and tumor weight at the endpoint of the experiment. Our data showed that auranofin treatment significantly reduced tumor weight in GO297 PDX compared with vehicle-treated tumors (Figure 1H). However, auranofin had negligible anti-tumor activity in MYC-low LP28 HGSOC PDXs (Figure 1H), suggesting that auranofin exerts significant anti-cancer activity in MYC-high HGSOCs *in vivo*.

The redox proteome identifies multiple pathways altered by auranofin in MYC-high HGSOC cells

Auranofin-induced TrxR1 inhibition is known to increase intracellular oxidative stress levels in cancer cells,[9,39] which may alter the redox status of multiple key signaling proteins or pathways, including NF-kβ and AP-1.[40] To interrogate the molecular mechanism underlying auranofin sensitivity in MYC-high HGSOC cells, we generated simultaneous expression and cysteine redox-proteome profile of MYC-high OVCAR-8 cells treated with DMSO or 2.5 μM auranofin for 8 h followed by sequential iodoTMT labeling.[41] As such, redox measurements, including oxidized proteins and reduced proteins, were normalized to total protein abundance. Cysteine redox proteome allows the mapping of oxidation or reduction state of proteins containing redox-sensitive cysteine residues.[42] Within 8 h of treatment, we observed an increase in the oxidation level of multiple peptides (Figure 2A) in response to auranofin compared with the DMSO control samples. In total, 5,353 iodoTMT-containing peptides were quantified, of which 5,276 peptides corresponding to 2,054 unique proteins considered for the experimental analysis after contaminants were removed. We identified 290 oxidized proteins and 175 reduced proteins after 8-h auranofin treatment (absolute fold change > 2, adjusted $p < 0.05$) (Figure 2B; Table S2). We found TrxR1 to be significantly oxidized on auranofin treatment, serving as an internal positive control (Figure 2B).

To further understand the cellular pathways perturbed by auranofin-induced oxidation, we performed Kyoto Encyclopedia of Genes and Genomes (KEGG) pathway analysis using the DAVID Functional Annotation tool.[43,44] The analysis indicated that components of spliceosome, proteasome, ribosome, RNA transport, focal adhesion, glycolysis/gluconeogenesis, protein processing in endoplasmic reticulum (ER), and DNA repair were significantly oxidized (Figure 2C). Because MYC regulates glycolysis to fuel cancer cells for survival,[4] we next examined the oxidation state of glycolysis proteins on auranofin treatment. Interestingly, we found that multiple components of glycolysis proteins were significantly oxidized (Figures 2B and 2E), including GAPDH (oxidation ratio [OD] of 2.8; $p = 0.0003$) being the primary target, followed by PGAM1 (OD of 2.7; $p = 0.0003$), PGK1 (OD of 2.6; $p = 0.0017$), TPI1 (OD of 2.5; $p = 0.0012$), ALDH7A1 (OD of 1.95; $p = 0.0003$), and ALDOA (OD of 1.8; $p = 0.0017$) (Figure 2D).

Auranofin inhibits glycolysis in MYC-high HGSOC cells

Because MYC-high HGSOC cells are more sensitive to auranofin and auranofin inhibits the glycolysis pathway in these cells (Figure 2), we examined the enrichment of glycolysis-regulated genes in MYC-high and -low HGSOCs using the TCGA dataset. We found that MYC-high HGSOCs have enrichment in a glycolysis gene signature (Figure 3A), suggesting that these tumors rely on glycolysis to fuel their energy demand for survival and growth. We then validated these findings by measuring cellular glucose uptake in HGSOC lines. Both MYC-high-expressing OVCAR-8 and PEO1 cells have higher glucose uptake compared with MYC-low-expressing OVCAR-4 and PEO4 cells (Figure 3B), suggesting that MYC-high HGSOC cells consume high glucose to fuel the glycolytic pathway for survival.

Because GADPH is a key rate-limiting enzyme in glycolysis and is oxidized in response to auranofin treatment (Figures 2 and 3C), we first measured GAPDH enzymatic activity in MYC-high OVCAR-8 and MYC-low OVCAR-4 cells after auranofin treatment (2.5 μM, 24 h). Auranofin significantly inhibited GAPDH enzymatic activity in OVCAR-8 cells, but an opposite trend was observed in OVCAR-4 cells (Figure 3D). Lactate is the end-product metabolite of the glycolysis pathway (Figure 3C), and hence is the functional readout

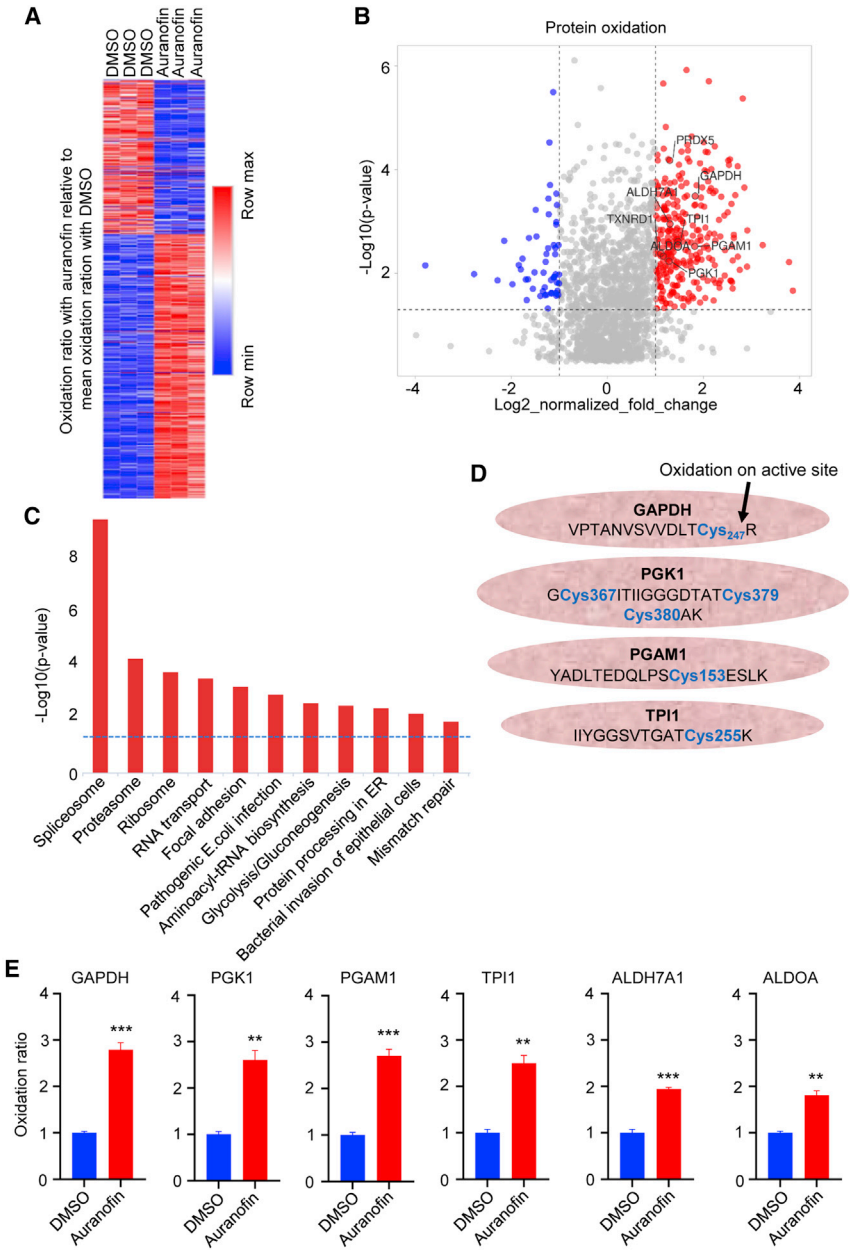

Figure 2. The redox proteome of MYC-high HGSOC cells after auranofin treatment

OVCAR-8 cells were treated with auranofin (2.5 μM) for 8 h. Auranofin-induced global cellular redox alterations were analyzed by cysteine redox proteomics using iodoTMT labeling. (A) The oxidation level of peptides is plotted as oxidation ratio on auranofin treatment relative to the mean oxidation ratio on DMSO treatment. (B) Volcano plot showing the proteins that were either oxidized (in red) or reduced (in blue) in response to auranofin treatment compared with DMSO control (Log2Fold change). (C) Top oxidized proteins were analyzed with Functional Annotation Clustering tool in DAVID. Top enriched biological pathways with minimal redundancy ($p < 0.05$) are shown (n = 3). (D) Oxidation of cysteine residues on active sites of glycolysis proteins, including GAPDH, PGK1, PGAM1, and TPI1. (E) Oxidation of glycolysis proteins, including GAPDH1, PGK1, PGAM1, TPI1, ALDH7A1, and ALDOA, is shown. Student's t test ($p < 0.05$) (mean ± SD).

to measure glycolysis in cells. Although intracellular glucose uptake and levels did not change significantly on auranofin treatment in these cells (Figure S4A), we found a significant reduction in extracellular lactate concentration in MYC-high cells, whereas no negligible effect was seen in MYC-low cells (Figure 3E). Likewise, targeted central carbon metabolomics analysis of MYC-high OVCAR-8 cells revealed increased intracellular concentrations of glycolytic metabolites upstream of GAPDH and decreased intracellular concentration of a glycolytic metabolite downstream of GAPDH, pyruvic acid, as a likely consequence of auranofin-induced GAPDH inhibition in OVCAR-8 cells (Figure 3F; Table S3). In contrast, no significant change in intracellular concentrations of metabolites upstream or downstream of GAPDH, except glycerol 3-phosphate, was observed in MYC-low PEO4 cells (Figure S4B; Table S3). Taken together, our results suggest that auranofin inhibits the glycolysis pathway in MYC-high HGSOC cells via GAPDH inhibition.

Auranofin increases glutamine metabolism in MYC-high HGSOC cells

To sustain survival, cancer cells can switch to alternate metabolic pathways in response to inhibition of a particular metabolic process. Although auranofin reduced tumor growth in MYC-high GO297 HGSOC PDXs *in vivo*, it failed to completely regress tumor growth (Figure 1F). We hypothesized that the residual cells may have switched to an alternate metabolic pathway for survival in response to auranofin treatment. Other than glycolysis, the glutamine metabolism is another key metabolic pathway essential for cancer cell survival.[20] Glutamine is a nonessential amino acid but can be transported into cells through many transporters, and MYC-high cells have been shown to have conditional dependency on exogenous sources of glutamine in addition to glycolysis.[45–47] The glutaminase pathway takes up glutamine from the microenvironment and converts it to glutamate through the enzymatic activity of the glutaminase GLS1, which will then feed into the TCA cycle. MYC transcriptionally regulates the key components of the glutaminase metabolic pathway.[46]

Next, we investigated whether MYC-high HGSOC cells could completely switch to glutamine metabolism for survival in response

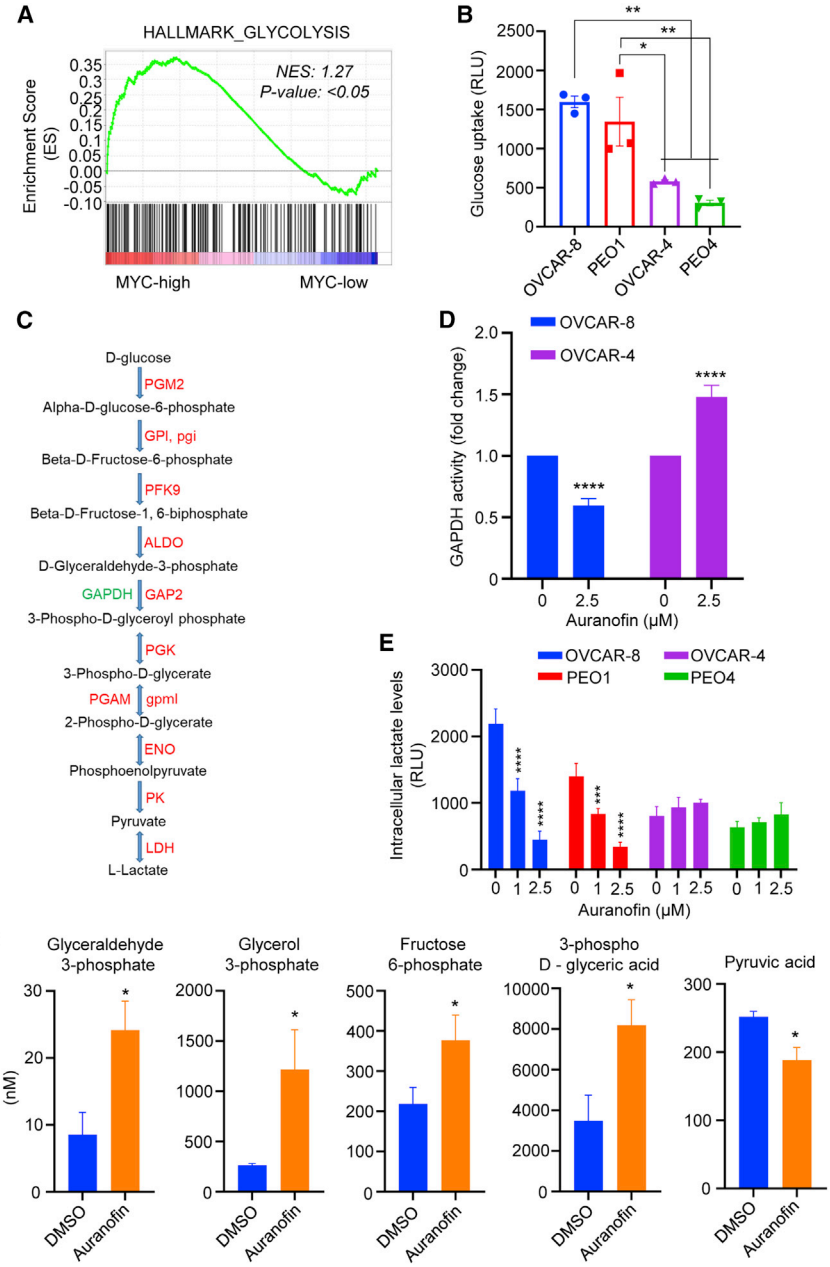

Figure 3. Auranofin inhibits glycolysis in MYC-high HGSOC cells

(A) Enrichment of glycolysis gene signature in MYC-high ovarian cancer patients compared with MYC-low ovarian cancer patients as analyzed using the TCGA dataset. Patients were divided into two groups based on the median MYC expression. Black bars at the bottom represent the genes belonging to the glycolysis pathway. Color bar at the bottom represents patients with high MYC expression (red) to patients with low MYC expression (blue). (B) Intracellular glucose uptake in two MYC-high lines (OVCAR-8 [blue] and PEO1 [red]) and two MYC-low HGSOC lines (OVCAR-4 [purple] and PEO4 [green]) was analyzed. One-way ANOVA followed by Tukey's post-test ($p < 0.05$, n = 3, mean ± SEM). (C) Glycolysis pathway highlighting each catalytic step, glycolytic metabolites, and key rate-limiting enzymes catalyzing each conversion step. (D) OVCAR-8 (blue) and OVCAR-4 (purple) cells were treated with auranofin (0–2.5 μM) for 24 h, and intracellular GAPDH enzyme activity was analyzed. One-way ANOVA followed by Tukey's post-test ($p < 0.05$, n = 3, mean ± SD). (E) Two MYC-high (OVCAR-8 and PEO1) and two MYC-low (OVCAR-4 and PEO4) cells were treated with auranofin (0–2.5 μM) for 24 h, and intracellular lactate levels were analyzed. One-way ANOVA followed by Tukey's post-test ($p < 0.05$, n = 3, mean ± SD). (F) OVCAR-8 cells, treated either with DMSO or 2.5 μM auranofin for 24 h, were then subjected to targeted central carbon metabolomics using LC/MS-MS. Intracellular concentrations of key glycolytic metabolites, both upstream and downstream of GAPDH, are shown. Student's t test ($p < 0.03$, n = 3, mean ± SEM).

to auranofin-induced glycolysis inhibition. We first analyzed the expression of GLS1 protein, a crucial regulator of glutamine catabolism, and observed an increased GLS1 protein level on auranofin treatment in MYC-high cells (OVCAR8, PEO1, DF149) but negligible change in MYC-low cells (OVCAR4 and PE04) (Figure 4A), suggesting that MYC-high HGSOC cells may switch to glutamine metabolism on auranofin treatment. We next measured the amount of glutamine and glutamate in cell culture media on auranofin treatment (2.5 μM, 24 h) in MYC-high and -low HGSOC lines. Auranofin significantly reduced glutamine levels (Figure 4B) and increased glutamate levels (Figure 4C) in the media of MYC-high HGSOC cells. No significant change in glutamine and glutamate levels was observed in the media of auranofin-treated MYC-low HGSOC cells (Figures 4B and 4C). Likewise, auranofin treatment significantly reduced glutamine levels and increased glutamate levels in the media of MYC-high patient-derived HGSOC cells, but not in MYC-low patient-derived cells (Figures 4D and 4E). Increased intracellular glutamate is a precursor for glutathione (GSH) synthesis, which is carried out by two conjugation reactions catalyzed by glutamate cysteine ligase and GSH synthase.[48] Intracellular glutamate is exported out of the cells through the amino acid transport system x_c^- coupled to the influx of extracellular cystine, which serves as a precursor for GSH synthesis.[49] We, therefore, measured intracellular GSH levels in auranofin-treated cells. Auranofin significantly increased in intracellular GSH levels in both MYC-high OVCAR-8 and PEO1 cells, but not in MYC-low OVCAR-4 and PEO4 cells (Figure 4F). Similarly, auranofin treatment also increased intracellular GSH levels in patient-derived MYC-high DF149 cells *ex vivo* (Figure 4G).

Auranofin increases intracellular ROS levels,[9] and increased ROS is known to upregulate GLS1 and glutamine metabolism.[50] We next

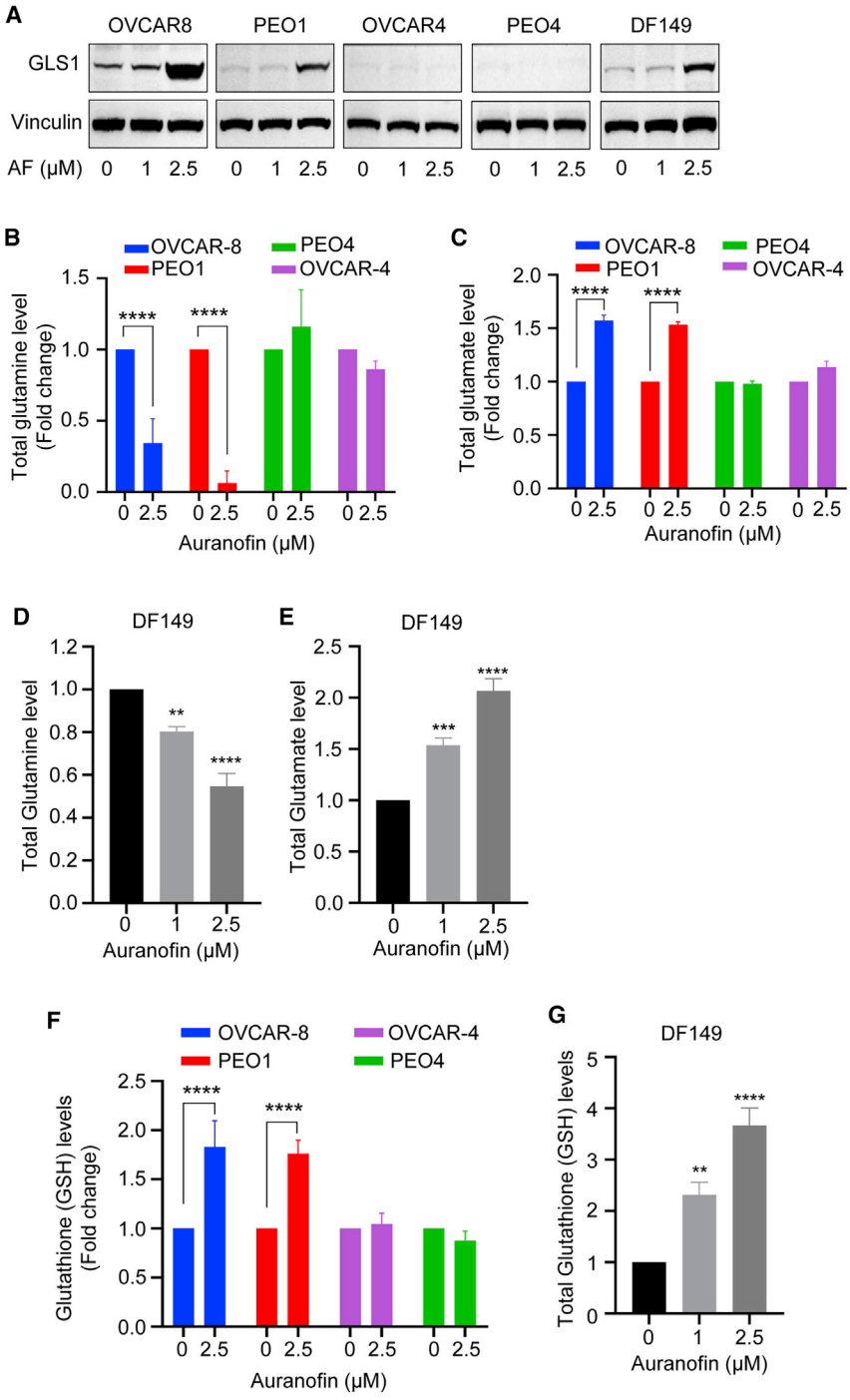

Figure 4. Auranofin upregulated glutamine metabolism in MYC-high HGSOC cells

(A) OVCAR-8, PEO1, OVCAR-4, PEO4, and DF149 cells were treated with auranofin (0–2.5 μM) for 24 h. GLS1 protein levels were then analyzed by western blot analysis; n = 3. (B and C) Two MYC-high (OVCAR-8 [blue] and PEO1 [red]) and two MYC-low (OVCAR-4 [purple] and PEO4 [green]) cells were treated with DMSO or auranofin (2.5 μM) for 24 h. The amount of glutamine (B) and glutamate (C) in the media of each treated and untreated line were analyzed. Two-way ANOVA followed by Sidak's post-test ($p < 0.05$, n = 3, mean ± SD). (D and E) MYC-high patient-derived HGSOC tumor cells DF149 were treated either with DMSO or auranofin (2.5 μM) for 24 h. The amount of glutamine (D) and glutamate (E) in the media of each treated and untreated line were analyzed. One-way ANOVA followed by Tukey's post-test ($p < 0.05$, n = 3, mean ± SD). (F and G) OVCAR-8, PEO1, OVCAR-4, PEO 4 (F), and DF149 (G) cells were treated with or without auranofin for 24 h, and intracellular glutathione (GSH) levels were then analyzed. Two-way ANOVA for cell lines and one-way ANOVA for DF149 cells ($p < 0.05$, n = 3, mean ± SD).

sought to determine whether auranofin would increase glutamine metabolism in a ROS-dependent manner. We found that pre-treatment of HGSOC cells with ROS scavenger *N*-acetyl-cysteine (NAC) abolished auranofin-induced GLS1 upregulation in OVCAR-8 cells (Figure S5A), abolished auranofin-induced reduction in glutamine levels in culture media, and also reversed auranofin-induced increase in glutamate levels in culture media (Figures S5B and S5C). Moreover, NAC pre-treatment also reversed the auranofin-induced increase in the intracellular GSH levels in both MYC-high OVCAR-8 and PEO1 cells (Figure S5D). Hence our data indicated that auranofin increases cellular glutamine metabolism in a redox-dependent manner. Overall, our data suggest that MYC-high HGSOC cells switch to glutamine metabolism for survival in response to auranofin-induced glycolysis inhibition.

Auranofin exerts synergistic anti-cancer activity with glutaminase inhibitor CB-839 or glutamine starvation

Because auranofin treatment increases glutamine metabolism in MYC-high HGSOC cells, we hypothesized that inhibition of the glutamine metabolism using a specific glutaminase (GLS1) inhibitor, CB-839,[24] may sensitize MYC-high HGSOC cells to auranofin-mediated cell killing. To test this notion, we pre-treated MYC-high and -low HGSOC cell lines and patient-derived tumor cells with the glutaminase inhibitor CB-839 (100 nM) for 6 h followed by treatment with auranofin (0–1 μM) for a further 72 h. Interestingly, a synergistic cell growth inhibition (combination index < 1) was observed with combined CB-839-auranofin treatment in both MYC-high HGSOC cell lines (OVCAR-8 and PEO1) and patient-derived tumor cells (DF149 and DF68), but not in MYC-low HGSOC cells (Figures 5A, 5B, and S6A). This corresponds with a near-complete elimination

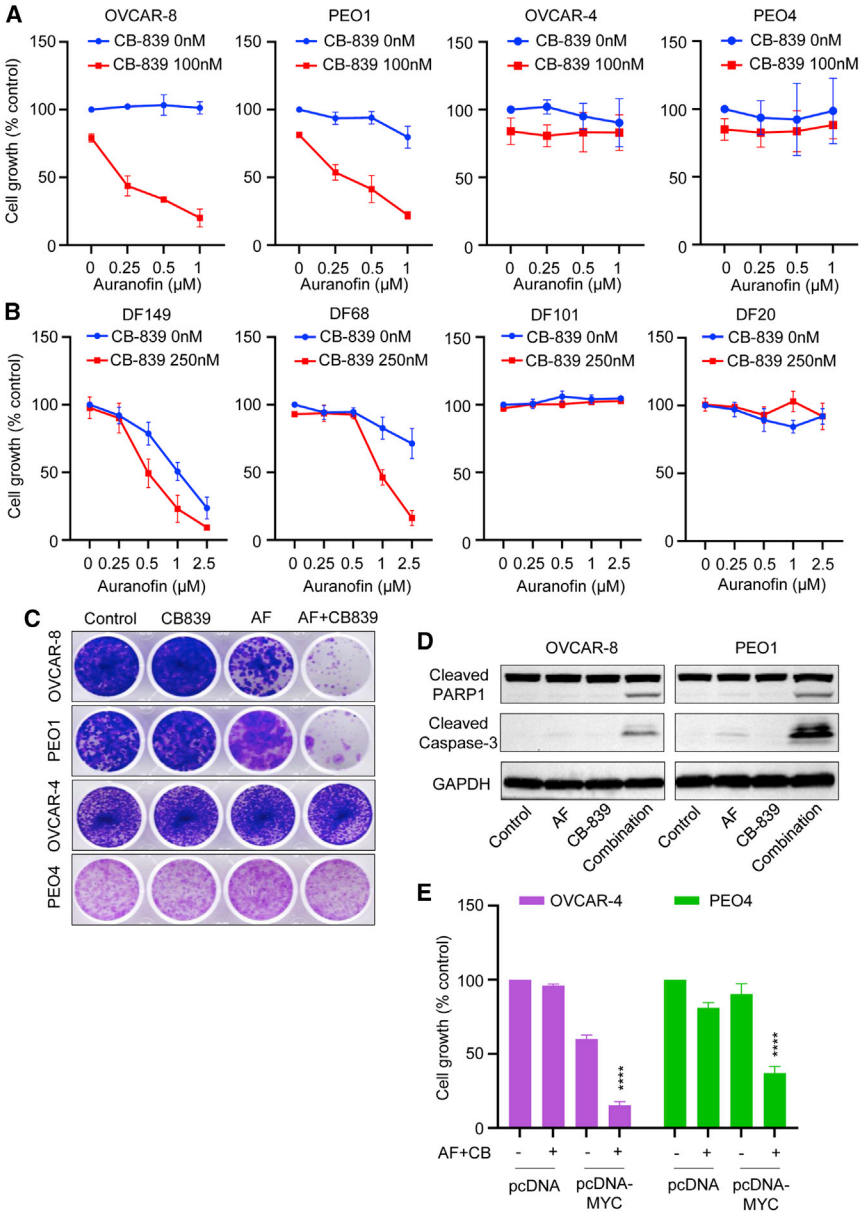

Figure 5. Auranofin exerts synergistic anti-cancer activity with glutaminase inhibitor CB-839

(A) Synergistic anti-cancer activity of CB-839 (100 nM) in combination with auranofin (0–1 μM) was analyzed after 72-h treatment on two MYC-high (OVCAR-8 and PEO1) and two MYC-low (OVCAR-4 and PEO4) lines. (B) Synergistic anti-cancer activity of CB-839 (250 nM) in combination with auranofin (0–1 μM) was analyzed after 72-h treatment on two MYC-high (DF149 and DF68) and two MYC-low (DF101 and DF20) patient-derived HGSOC tumor cells. Two-way ANOVA followed by Sidak's post-tests ($p < 0.05$, n = 3, mean ± SD). (C) Representative images of colony-forming capacity of OVCAR-8, PEO1, OVCAR-4, and PEO4 cells following the treatment with CB-839 (500 nM) and auranofin (1 μM), both alone and in combination, at 14 days analyzed using crystal violet staining (n = 3). (D) OVCAR-8 and PEO1 cells were treated with auranofin and CB-839, both alone and in combination, for 24 h, and caspase-3 and PARP1 cleavage were examined by western blot analysis. (E) Effect of auranofin (1 μM) and CB-839 (250 nM) treatment (72 h), both alone and in combination, on OVCAR-4 (purple) and PEO4 (green) endogenously overexpressing MYC was analyzed using crystal violet staining. Two-way ANOVA followed by Sidak's tests ($p < 0.05$, n = 3, mean ± SD).

of colony-forming capacity on CB-839-auranofin combination treatment in MYC-high HGSOC cells, but not in MYC-low HGSOC cells (Figure 5C). Additionally, we also observed that auranofin and CB-839 combination treatment sensitized MYC-high cells to caspase-3-dependent apoptosis as assessed by cleavage of caspase-3 and its substrate, PARP1 (Figure 5D), while either auranofin or CB-839 alone showed minimal induction of cell death. Next, we assessed the synergistic anti-cancer activity of TrxR1 inhibition and CB-839 using more a specific TrxR1 inhibitor, TRi-1. Similar to auranofin, TRi-1 exerted synergistic anti-cancer activity with CB-839 in MYC-high OVCAR-8 and PEO1 cells, but not in MYC-low OVCAR-4 and PEO4 HGSOC cells (Figure S6B). We also observed that TRi-1 and CB-839 combination treatment sensitized MYC-high cells to caspase-3-dependent apoptosis as assessed by cleavage of caspase-3 and PARP1 (Figure S6C).

Because auranofin and CB-839 combination treatment selectively induced a growth-suppressive effect in MYC-high HGSOC cells, we further investigated whether ectopic expression of MYC in MYC-low-expressing OVCAR-4 and PEO4 cells would sensitize to combination treatment. To test this, we overexpressed MYC in low-MYC HGSOC lines for 24 h, followed by treatment with drug combination for a further 72 h. MYC overexpression significantly sensitized both OVCAR-4 and PEO4 cells to auranofin and CB-839 combination therapy compared with pcDNA vector-transfected control cells (Figure 5E). Taken together, our data strongly suggest that auranofin exerts synergistic anti-cancer activity with glutamine pathway inhibitor CB-839 in MYC-high HGSOC cells.

To further confirm the role of glutamine metabolism on conferring resistance to auranofin treatment, we depleted glutamine from cell culture media for 16 h followed by auranofin treatment for a further 72 h. As a positive control, we also supplemented glutamine-free media with 4 mM L-glutamine and treated the cells with auranofin for 72 h. Interestingly, glutamine starvation significantly sensitized MYC-high OVCAR-8 and PEO1 cells to auranofin treatment

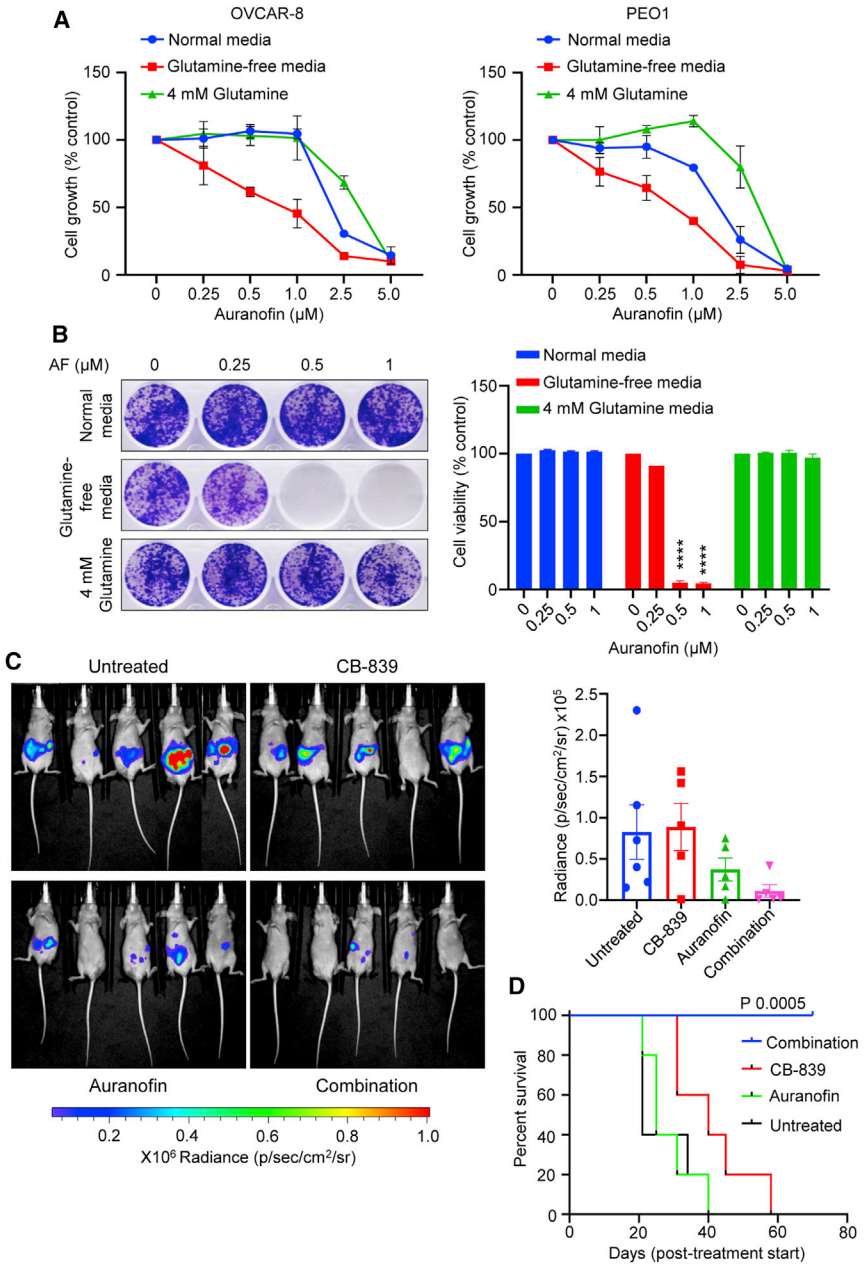

Figure 6. Glutamine depletion sensitizes MYC-high HGSOC cells to auranofin

(A) OVCAR-8 and PEO1 cells were cultured either in normal growth media, glutamine-free growth media, or glutamine-free media supplemented with 4 mM L-glutamine 16 h prior to auranofin treatment (0–5 μM) in respective media for 72 h. Cell proliferation of each cell line under each growth condition was analyzed. Two-way ANOVA followed by Sidak's post-tests ($p < 0.05$, n = 3, mean ± SD). (B) OVCAR-8 cells were cultured in normal growth media, glutamine-free media, and glutamine-free media supplemented with 4 mM L-glutamine for 16 h prior to auranofin treatment (0–1 μM) for 24 h. One thousand cells from each treatment condition were seeded onto 12-well plates for clonogenic survival. Representative images of colony-forming capacity of OVCAR-8 cells at 14 days were analyzed using crystal violet staining (left panel). Quantification of the colonies formed in OVCAR-8 cells measured by reading crystal violet absorbance (right panel). Two-way ANOVA followed by Sidak's post-test ($p < 0.05$, n = 3, mean ± SD). (C) BALB/c Nude mice bearing luciferase-tagged OVCAR-8 tumor cells were treated with vehicle, auranofin (half-MTD, 5 mg/kg), CB-839 (half-MTD, 100 mg/kg), or a combination for 2 weeks (n = 5 mice in each treatment group). Tumor growth was monitored by bioluminescence imaging (mean ± SEM). Representative images and quantification analysis of tumor burden on days 0 and 15 (post-treatment start) are shown. (D) The Kaplan-Meier survival analysis of OVCAR-8 tumor-bearing BALB/c nude mice after treatment with vehicle, auranofin, CB-839, and a combination.

(Figure 6A), but not MYC-low OVCAR-4 and PEO4 cells (Figure S7). Notably, the clonogenic potential of MYC-high OVCAR-8 cells was markedly abolished on combined glutamine starvation with auranofin treatment (Figure 6B). We observed that glutamine depletion itself partly reduced proliferation of MYC-high OVCAR-8 cells, but not the proliferation of MYC-high PEO1 cells (data not shown). Taken together, our data indicated that glutamine metabolism plays a crucial role in making cells resistant to auranofin treatment, and that the cells switch to glutamine metabolism for survival when auranofin inhibits glycolysis in MYC-high HGSOC cells.

We next confirmed the *in vivo* anti-cancer activity of auranofin and CB-839 combination therapy using luciferase-tagged OVCAR-8 xenograft. Luciferase-tagged MYC-high OVCAR-8 cells were engrafted into BALB/c Nude mice intraperitoneally (i.p.) and treated with auranofin and CB-839 alone or in combination. Our results showed that CB-839 monotherapy had no effect on tumor growth. However, auranofin monotherapy partially reduced tumor burden in mice. Interestingly, although not statistically significant because of variation in tumor growth in each treatment group, auranofin and CB-839 combination therapy completely regressed the tumor in three of five mice and partially reduced tumor burden in two of five mice (Figure 6C). We have then followed these mice for the Kaplan-Meier survival analysis for 70 days. The median survival was observed to be 21 days in vehicle-treated mice, 25 days in CB-839-treated mice, and 40 days in auranofin-treated mice. Although auranofin treatment partially reduced tumor burden in mice, tumors regrew rapidly on treatment withdrawal, resulting in shorter survival. Interestingly, all mice from the auranofin and CB-839 combination treatment group were

disease free and alive to the end of an experiment, and combination treatment has prolonged the survival of mice to 70 days (log rank $p < 0.05$; Figure 6D). Hence our data indicated that auranofin and CB-839 combination therapy exerts significant anti-cancer activity and prolonged the survival of tumor-bearing mice *in vivo*.

DISCUSSION

In this study, we aimed to identify a novel effective therapeutic strategy against MYC-high HGSOCs, which are usually detected with widespread dissemination at the time of presentation and resulting in poor overall prognosis. Although MYC represents an attractive drug target because of its role in tumorigenesis, including in HGSOC, drugs directly targeting MYC have failed in clinical trials. Here, we discovered an upregulated thioredoxin system as a new target in MYC-driven HGSOCs. MYC-high tumors are known to have an increased level of ROS and might therefore have increased survival dependency on antioxidant defense systems. The thioredoxin system, a crucial redox regulator, is involved in regulating a number of redox-sensitive factors and key rate-limiting enzymes required for various cellular processes.[40] In this study, we identified increased expression of TrxR1 as a potential therapeutic vulnerability in MYC-high HGSOCs, which can be exploited using the FDA-approved TrxR1 inhibitor auranofin. Auranofin is a gold-based compound that inhibits TrxR1 redox activity, is FDA approved for rheumatoid arthritis patients, and has received increasing attention as a potential anticancer drug.[9,51,52] We demonstrate that auranofin selectively inhibits growth and induces apoptosis in MYC-high HGSOC cells compared with MYC-low HGSOC cells both *in vitro* and *in vivo*.

Auranofin is a redox-modulating molecule; several studies have used redox proteomics to map the effect of auranofin-induced oxidative stress on various signaling molecules.[41,53] Auranofin inhibits TrxR1 redox activity via irreversible binding to selenocysteine residue present in the C-terminal domain. Auranofin inhibits AKT signaling by oxidizing Cys60 and Cys77, which is required for AKT recruitment onto plasma membrane.[53] Auranofin, along with more specific TrxR1 inhibitors, TRi-1 and TRi-2, has been profiled using redox proteomic, and a number of proteins belonging to glycolysis, TCA cycle, carbon metabolism, ribosome biogenesis, and spliceosome were oxidized.[37] Similarly, auranofin has been shown to change expression and oxidation of similar key signaling pathways, including oxidative phosphorylation and glycolysis in OC cell line A2780.[54] Using the redox proteomic approach, we mapped the effect of auranofin on oxidation status of proteins in MYC-high HGSOC cells. We demonstrated that auranofin oxidized several key proteins belonging to various cellular processes, including spliceosome, proteasome, ribosome biogenesis, RNA transport, glycolysis, and mismatch repair. In contrast with previous study in A2780 OC cells where auranofin was shown to predominantly oxidize proteins belonging to the oxidative phosphorylation pathway, we observed no defects in the oxidative phosphorylation pathway, but only observed oxidation of a number of glycolysis proteins. This could be explained based on the fact that A2780 cells are not high-grade serous OCs.[55] MYC transcriptionally regulates multiple metabolism pathways, including glycolysis.[4] Our redox proteomics data revealed that auranofin oxidizes several key glycolysis rate-limiting enzymes, including GAPDH. Auranofin oxidizes surface-exposed Cys247 present in the catalytic active sites in GAPDH, oxidative modification of which results in its impaired catalytic and glycolytic activity.[56] In line with this study, we demonstrated that auranofin inhibits GAPDH enzyme activity, reduces intracellular lactate and pyruvate concentrations, and increases intracellular concentrations of glycolysis metabolites upstream of GAPDH in MYC-high HGSOC cells. Our findings demonstrated a novel mechanism underlying anti-cancer activity of auranofin by inhibiting glycolysis in a redox-dependent manner in MYC-high HGSOC cells.

Tumor cells often undergo metabolic rewiring on inhibition of one key cellular metabolic pathway and switch to an alternate metabolic pathway to fulfill their high-energy demand. In addition to regulating glycolysis pathway genes, MYC also transcriptionally regulates glutamine pathway genes, and inhibition of the glutamine pathway has shown synthetic lethality in MYC-high OCs.[5,46] In this study, we demonstrated that auranofin-induced glycolysis inhibition leads to upregulation of glutamine metabolism only in MYC-high HGSOC cells and not in MYC-low HGSOC cells. These findings suggested a potential role of glutamine metabolism as a resistance mechanism to auranofin in MYC-high HGSOC cells. This hypothesis could be well explained by generating auranofin-resistant HGSOC cells and examining glutamine metabolism status in resistant cells compared with parental HGSOC cells. We also observed increased intracellular levels of reduced GSH in MYC-high HGSOC cells on auranofin treatment, which was due to an increased glutamine metabolism. Such upregulation of GSH, another major cellular antioxidant system, may protect HGSOC cells from increased oxidative stress in response to auranofin-induced ROS. Inhibition of the thioredoxin system has been shown to induce the GSH system, and co-inhibition on both thioredoxin and the GSH system synergistically kills tumor cells.[57] However, the exact mechanism by which these two systems crosstalk is unknown. Our findings in this study provide a novel mechanistic insight on crosstalk between thioredoxin and the GSH system. Increased glutamine metabolism in response to auranofin-induced thioredoxin inhibition generates glutamate that can be exchanged for cystine via SLC7A11, and this cystine then serves as a precursor for GSH synthesis.

We discovered that dual targeting of TrxR1 using auranofin and a glutaminase inhibitor, CB-839, to inhibit glutamine metabolism produces a synergistic and selective anticancer effect on MYC-high HGSOC cells *in vitro*. CB-839 has shown promising anti-tumor activity in multiple human cancer models via glutamine metabolism inhibition.[24,58,59] The reason underlying the different sensitivity of MYC-high and MYC-low to auranofin and to the auranofin/CB-839 combination could be multifactorial. Of note, the NRF2 gene signature, a key transcriptional regulator of oxidative stress response, is constitutively upregulated in MYC-high tumors. The sustained induction of NRF2-target genes, including TrxR1, to counteract high endogenous ROS in MYC-high HGSOCs could explain cellular dependency on TrxR1 and thus sensitivity to auranofin and

auranofin/CB-839 combination through a further increase in ROS levels. A clinically relevant observation made in our study is that auranofin selectively inhibits glycolysis in MYC-high HGSOCs and conditions these cells to increase reliance on glutamine metabolism for maintaining cellular energy demand and redox homeostasis. Supporting this view, co-inhibition of GLS1 and TrxR1 compromised glutamine metabolism and redox homeostasis in favor of increased oxidative stress and cell death in MYC-high HGSOC cells.

Both auranofin and CB-839 are individually being tested in multiple phase I/II clinical trials on advanced solid cancers and hematological malignancies. Auranofin is an FDA-approved drug; its safety profile in humans is readily available, and CB-839 has been well tolerated in patients with minimal toxicities (ClinicalTrials.gov: NCT02861300). Our study provides a strong rationale for translating auranofin and CB-839 combination therapy in MYC-high HGSOC patients. Future studies are also needed to evaluate other tumors with MYC pathway activation in which a synergistic anti-cancer effect can be observed. Importantly, our study characterized TrxR1 as a biomarker, demonstrating auranofin and CB-839 synergistic activity only in MYC-high tumors can identify patients who are most likely to benefit from auranofin-CB-839 combination treatment. However, for clinical translation of our findings, it is necessary to identify robust markers to stratify patients into MYC-high and MYC-low groups to reflect the biological effect of auranofin and CB-839 combination therapy. Further studies are required to identify such biomarkers to help identify the MYC-high patients who are likely to respond to auranofin and CB-839 combination therapy.

MATERIALS AND METHODS

Cell lines and reagents

HGSOC cell lines, including OVCAR-8, OVCAR-4, OVCAR-3, and OAW42, were kindly provided by Dr. Elaine Sanij (St. Vincent's Hospital). HGSOC cell lines, including PEO1, PEO4, SKOV3, and JAM, were from American Type Culture Collection (ATCC; Manassas, VA, USA). Cell lines were cultured in RPMI 1640 media containing 10% fetal bovine serum (FBS) (Gibco). All cell lines were tested for Mycoplasma infection and authenticated using short tandem repeat (STR) profiling by scientific services at QIMR Berghofer Medical Research Institute. Auranofin was purchased from Cayman Chemicals (catalog number [Cat #]: 15316). CB-839 was purchased from Selleck Chemicals (Cat #: S7655). Sodium selenite was purchased from Sigma (Cat #: S5261).

Patient-derived tumor cells/PDXs

Ascites-derived HGSOC PDX models, including DF20, DF68, DF86, DF101, DF106, DF149, and DF181, were obtained from the Dana-Farber Cancer Institute, USA.[60] All of these PDXs were expanded and passaged into 6-week-old female NRG (NOD/RAG1/2$^{-/-}$/IL2R$\gamma^{-/-}$) mice and banked for future use for *in vivo* and *ex vivo* studies. Ascites-derived HGSOC patient-derived tumor cells described above were cultured and maintained in RPMI 1640 medium containing 10% FBS for short-term culture, at 37°C with 5% CO2 for *ex vivo* experiments.

TCGA dataset analysis

Gene expression data for the TCGA-OV dataset were downloaded using the Genomic Data Commons (GDC) portal (https://portal.gdc.cancer.gov/, accessed on January 21, 2021). Primary tumor samples were used for the analysis. The entire sample set was divided into two groups, High MYC (187 samples) and Low MYC (187 samples) groups, using the median MYC normalized expression (FPKM count) value as cutoff. Differential gene expression analysis was performed between the two groups using the R package edgeR.[61] The genes were ranked using the formula −log10 (p value)*sign [fold change (FC)]. The GSEA pre-ranked analysis was performed on the ranked genes using the GSEA software (v.4.1.0) and MSigDB.[62–64]

Redox proteomics

Sample preparation

Sample preparation for redox proteomics was carried out as described previously.[41,53] In brief, OVCAR-8 cells were treated with 2.5 μM auranofin for 8 h, and cells were trypsinized and counted. An equal number of control and auranofin-treated OVCAR-8 (2×10^6) cells were lysed in 2% SDS containing 50 mM tri-ethyl ammonium bicarbonate (TEABC) and sonication. Approximately 300 μg of protein from each condition was alkylated with 100 mM iodoacetamide (IAA) at room temperature for 40 min in the dark. Excess IAA was removed by buffer exchange with HEPES-EDTA-Sucrose (HES) buffer using 30-kDa molecular mass cutoff filters. Protein concentrations were estimated using the bicinchoninic acid assay and adjusted to 1 μg/μL. To each 100-μg sample, 1 μL 0.5 M Tris(2-carboxyethyl) phosphine hydrochloride (TCEP) was added and reduced at 50°C for 1 h. IodoTMT labeling was then carried out, and excess labels were quenched by adding dithiothreitol to a final concentration of 20 mM and incubating for 15 min at 37°C in the dark. Equal amounts of each labeled sample were combined, and acetone was precipitated overnight. The protein pellet was resuspended in 50 mM triethyl ammonium bicarbonate buffer and digested with LysC for 2 h at 30°C. Trypsin (Promega) was added to the protein-LysC mixture at the ratio of 1:20 (enzyme: protein), and digestion was continued overnight at 37°C. The iodoTMT-labeled peptides were fractionated using high pH reverse-phase liquid chromatography[65] and concatenated into six fractions. The fractions were dried, desalted, and stored at −80°C until liquid chromatography-tandem mass spectrometry (LC-MS/MS) analysis. For total proteome analysis, an aliquot of protein lysate from each sample was reduced, alkylated, and digested. The reduction, alkylation, and enzymatic digestion conditions were identical to the iodoTMT experiment.

Mass spectrometry data acquisition

LC-MS/MS for iodoTMT and the total proteome samples were performed using a nanoAcquity UHPLC (Waters, Milford, MA, USA) system connected to a Orbitrap Fusion Tribrid mass spectrometer (Thermo-Fisher Scientific, Waltham, MA, USA). Peptides were reconstituted in 0.1% formic acid and were loaded onto an Acquity UPLC M-Class V/M symmetry trap column (Waters) at 5 μL/min before resolving with the analytical column (Acquity UPLC M-Class Peptide BEH C18 nanoAcquity column; Waters) over a

run time of 120 min. Separation of peptides was performed at 300 nL/min using a linear ACN gradient of buffer A (0.1% formic acid in water) and buffer B (0.1% formic acid in ACN). The column compartment was held at 45°C for the entire analysis.

Mass spectra were collected in data-dependent acquisition (DDA) mode. Both MS1 and HCD-MS2 spectra were collected in the Orbitrap. MS1 scan parameters were scan range of 350–1800 m/z, 60,000 resolution, maximum (max) injection time of 22 ms, and Automatic Gain Control (AGC) target 1e6. Dynamic exclusion parameters were set as follows: exclude isotope true, duration 30 s and using the peptide monoisotopic peak determination mode, charge states of 2–6 were included. Peptides were fragmented using stepped collision energy of 25, 30 and 35. MS2 spectra were collected at a resolution of 15K with an AGC target of 5e4, maximum ion injection time (IT) of 40 ms.

Mass spectrometry data processing

Raw data obtained from LC-MS/MS were searched against the UniProt human protein database using Sequest HT through Proteome Discoverer (Version 2.2) (Thermo Scientific, Bremen, Germany). Precursor and fragment mass tolerance were set to 10 ppm and 0.05 Da, respectively. For iodoTMT data, iodoTMT and carbamidomethylation of cysteine were set as variable modifications along with oxidation of methionine. For total proteome data, carbamidomethylation of cysteine was set as a fixed modification. A false discovery rate (FDR) threshold of 1% was used to filter peptide spectrum matches (PSMs). FDR was calculated using a decoy search. A Student's t test was utilized, and an adjusted p value of 0.05 and fold-change threshold of 2 were used to determine differentially oxidized peptides.

Central carbon targeted metabolomics

The intracellular levels of central carbon metabolites were measured by Metabolomics Australia as described previously.[66] OVCAR-8 and PEO4 cells were treated with 2.5 μM auranofin for 24 h. The intracellular metabolites were extracted in 2 mL 50% acetonitrile and transferred to 2-mL Eppendorf tubes. Samples were then vortexed for 30 s and incubated on ice for 10 min to cool down. This step was repeated three times, and samples were then centrifuged for 5 min at 5,000 × *g*. The supernatant-containing metabolites were then transferred to a clean 2-mL microcentrifuge tube and stored at −80°C. These samples were then freeze dried overnight and resuspended in 100 μL of water with 10 μM AZT as internal standard. These samples were then transferred to high-performance liquid chromatography (HPLC) glass inserts for analysis. Central carbon metabolites were analyzed by LC-MS/MS using a scheduled multiple reaction monitoring method as described previously.[66]

In vivo xenografts

All experiments were approved by the QIMR Berghofer Medical Research Institute Animal Ethics Committee and the University of Queensland Animal Ethics Committee. Patient tumors for generation of PDX models in mice were obtained with informed consent under a protocol approved by the Mater Health Services Human Research Ethics Committee and the University of Queensland Human Research Ethics Committee. For both GO297 and LP28 HGSOC PDXs, tumor slurry was injected into the i.p. cavity of 6-week-old female NSG mice. Once tumors became palpable in the peritoneal cavity, mice were randomized into two groups (six mice per group) and treated with vehicle control or auranofin (10 mg/kg, Monday–Friday) via i.p. injections for 2 weeks. At the end of the 2-week period, mice were euthanized, tumors were harvested, and tumor weights were recorded.

For OVCAR-8 xenograft, 2×10^6 luciferase-tagged OVCAR-8 cells were engrafted into the i.p. cavity of 6-week-old female BALB/c Nude mice. Tumor growth was monitored 7 days after engraftment using Xenogen IVIS Bioluminescence imaging. Once tumors were established, mice were randomized into four groups (five mice per group): (1) vehicle, (2) CB-839 alone (half maximum-tolerated dose [MTD] 100 mg/kg, daily, oral gavage), (3) auranofin alone (half-MTD, 5 mg/kg, i.p., Monday–Friday), and (4) combination. Mice were treated for 2 weeks. Tumor growth was monitored by bioluminescence imaging at the end of 2 weeks of treatment. The survival analysis was performed using the Kaplan-Meier survival analysis.

Statistical analysis

All values are presented as mean ± SEM or mean ± SD. Data were analyzed using GraphPad Prism 6 (GraphPad Software, CA, USA). Statistical significance was determined by one-way ANOVA followed by Tukey's post-test and two-way ANOVA followed by Sidak's post-test. All data are expressed as mean values ± SEM or mean ± SD. Where applicable, statistical significance is denoted by $^*p \leq 0.05$, $^{**}p \leq 0.01$, $^{***}p \leq 0.001$, and $^{****}p \leq 0.0001$.

DATA AVAILABILITY STATEMENT

The mass spectrometry redox proteomics data have been deposited to the Proteome Xchange Consortium via the PRIDE partner repository. The request for any material should be directed to Prof. Kum Kum Khanna.

SUPPLEMENTAL INFORMATION

Supplemental information can be found online at https://doi.org/10.1016/j.ymthe.2022.12.011.

ACKNOWLEDGMENTS

We thank the personnel of the TRI Animal facility and QIMRB Proteomic facilities for their expert technical assistance. This study was supported by Ovarian Cancer Research Foundation and National Breast Cancer Foundation conjoint grant (ID ONBCF-20-011) and National Health and Medical Research Council (NH&MRC) Program Grant (1017028 to K.K.K.).

AUTHOR CONTRIBUTIONS

P.V.R. contributed to study concept and design, acquisition of data, analysis, and interpretation of data. P.V.R., K.K.K., J.D.H., and M.K. contributed to experimental design, analysis, interpretation of

data, and writing of the manuscript. P.V.R. and Y.H. carried out the PDX work. K.K.D. and H.G. contributed to proteomic experiments and data analysis. X.L. and U.R.M. helped with western blot analysis. P.V. and C.M. analyzed the clinical data. All authors contributed to review and revision of this manuscript.

DECLARATION OF INTERESTS

The authors declare no competing interests.

REFERENCES

1. Siegel, R.L., Miller, K.D., and Jemal, A. (2017). Cancer statistics, 2017. CA. Cancer J. Clin. *67*, 7–30. https://doi.org/10.3322/caac.21387.
2. Konstantinopoulos, P.A., and Awtrey, C.S. (2012). Management of ovarian cancer: a 75-year-old woman who has completed treatment. JAMA *307*, 1420–1429. https://doi.org/10.1001/jama.2012.269.
3. The Cancer Genome Atlas Research Network, Berchuck, A., Birrer, M., Chien, J., Cramer, D.W., Dao, F., Dhir, R., DiSaia, P., Gabra, H., Glenn, P., Godwin, A.K., et al. (2011). Integrated genomic analyses of ovarian carcinoma. Nature *474*, 609–615. https://doi.org/10.1038/nature10166.
4. Tateishi, K., Iafrate, A.J., Ho, Q., Curry, W.T., Batchelor, T.T., Flaherty, K.T., Onozato, M.L., Lelic, N., Sundaram, S., Cahill, D.P., et al. (2016). Myc-driven glycolysis is a therapeutic target in glioblastoma. Clin. Cancer Res. *22*, 4452–4465. https://doi.org/10.1158/1078-0432.CCR-15-2274.
5. Shen, Y.A., Hong, J., Asaka, R., Asaka, S., Hsu, F.C., Suryo Rahmanto, Y., Jung, J.G., Chen, Y.W., Yen, T.T., Tomaszewski, A., et al. (2020). Inhibition of the MYC-regulated glutaminase metabolic axis is an effective synthetic lethal approach for treating chemoresistant ovarian cancers. Cancer Res. *80*, 4514–4526. https://doi.org/10.1158/0008-5472.CAN-19-3971.
6. Tang, Y.-C., Hsiao, J.-R., Jiang, S.-S., Chang, J.-Y., Chu, P.-Y., Liu, K.-J., Fang, H.-L., Lin, L.-M., Chen, H.-H., Huang, Y.-W., et al. (2021). c-MYC-directed NRF2 drives malignant progression of head and neck cancer via glucose-6-phosphate dehydrogenase and transketolase activation. Theranostics *11*, 5232–5247. https://doi.org/10.7150/thno.53417.
7. Hanahan, D. (2022). Hallmarks of cancer: new dimensions. Cancer Discov. *12*, 31–46. https://doi.org/10.1158/2159-8290.CD-21-1059.
8. Hanahan, D., and Weinberg, R.A. (2011). Hallmarks of cancer: the next generation. Cell *144*, 646–674. https://doi.org/10.1016/j.cell.2011.02.013.
9. Raninga, P.V., Lee, A.C., Sinha, D., Shih, Y.Y., Mittal, D., Makhale, A., Bain, A.L., Nanayakarra, D., Tonissen, K.F., Kalimutho, M., and Khanna, K.K. (2020). Therapeutic cooperation between auranofin, a thioredoxin reductase inhibitor and anti-PD-L1 antibody for treatment of triple-negative breast cancer. Int. J. Cancer *146*, 123–136. https://doi.org/10.1002/ijc.32410.
10. Raninga, P.V., Di Trapani, G., Vuckovic, S., Bhatia, M., and Tonissen, K.F. (2015). Inhibition of thioredoxin 1 leads to apoptosis in drug-resistant multiple myeloma. Oncotarget *6*, 15410–15424. https://doi.org/10.18632/oncotarget.3795.
11. Johnson, F.D., Ferrarone, J., Liu, A., Brandstädter, C., Munuganti, R., Farnsworth, D.A., Lu, D., Luu, J., Sihota, T., Jansen, S., et al. (2022). Characterization of a small molecule inhibitor of disulfide reductases that induces oxidative stress and lethality in lung cancer cells. Cell Rep. *38*, 110343. https://doi.org/10.1016/j.celrep.2022.110343.
12. Van Loenhout, J., Freire Boullosa, L., Quatannens, D., De Waele, J., Merlin, C., Lambrechts, H., Lau, H.W., Hermans, C., Lin, A., Lardon, F., et al. (2021). Auranofin and cold atmospheric plasma synergize to trigger distinct cell death mechanisms and immunogenic responses in glioblastoma. Cells *10*. https://doi.org/10.3390/cells10112936.
13. Freire Boullosa, L., Van Loenhout, J., Flieswasser, T., De Waele, J., Hermans, C., Lambrechts, H., Cuypers, B., Laukens, K., Bartholomeus, E., Siozopoulou, V., et al. (2021). Auranofin reveals therapeutic anticancer potential by triggering distinct molecular cell death mechanisms and innate immunity in mutant p53 non-small cell lung cancer. Redox Biol. *42*, 101949. https://doi.org/10.1016/j.redox.2021.101949.
14. Hou, G.X., Liu, P.P., Zhang, S., Yang, M., Liao, J., Yang, J., Hu, Y., Jiang, W.Q., Wen, S., and Huang, P. (2018). Elimination of stem-like cancer cell side-population by auranofin through modulation of ROS and glycolysis. Cell Death Dis. *9*, 89. https://doi.org/10.1038/s41419-017-0159-4.
15. Baccelli, I., Gareau, Y., Lehnertz, B., Gingras, S., Spinella, J.F., Corneau, S., Mayotte, N., Girard, S., Frechette, M., Blouin-Chagnon, V., et al. (2019). Mubritinib targets the electron transport chain complex I and reveals the landscape of OXPHOS dependency in acute myeloid leukemia. Cancer Cell *36*, 84–99.e8. https://doi.org/10.1016/j.ccell.2019.06.003.
16. Raninga, P.V., Lee, A., Sinha, D., Dong, L.F., Datta, K.K., Lu, X., Kalita-de Croft, P., Dutt, M., Hill, M., Pouliot, N., et al. (2020). Marizomib suppresses triple-negative breast cancer via proteasome and oxidative phosphorylation inhibition. Theranostics *10*, 5259–5275. https://doi.org/10.7150/thno.42705.
17. Hensley, C.T., Wasti, A.T., and DeBerardinis, R.J. (2013). Glutamine and cancer: cell biology, physiology, and clinical opportunities. J. Clin. Invest. *123*, 3678–3684. https://doi.org/10.1172/JCI69600.
18. Wang, J.B., Erickson, J.W., Fuji, R., Ramachandran, S., Gao, P., Dinavahi, R., Wilson, K.F., Ambrosio, A.L.B., Dias, S.M.G., Dang, C.V., and Cerione, R.A. (2010). Targeting mitochondrial glutaminase activity inhibits oncogenic transformation. Cancer Cell *18*, 207–219. https://doi.org/10.1016/j.ccr.2010.08.009.
19. Mohamed, A., Deng, X., Khuri, F.R., and Owonikoko, T.K. (2014). Altered glutamine metabolism and therapeutic opportunities for lung cancer. Clin. Lung Cancer *15*, 7–15. https://doi.org/10.1016/j.cllc.2013.09.001.
20. Altman, B.J., Stine, Z.E., and Dang, C.V. (2016). From Krebs to clinic: glutamine metabolism to cancer therapy. Nat. Rev. Cancer *16*, 749. https://doi.org/10.1038/nrc.2016.114.
21. Seltzer, M.J., Bennett, B.D., Joshi, A.D., Gao, P., Thomas, A.G., Ferraris, D.V., Tsukamoto, T., Rojas, C.J., Slusher, B.S., Rabinowitz, J.D., et al. (2010). Inhibition of glutaminase preferentially slows growth of glioma cells with mutant IDH1. Cancer Res. *70*, 8981–8987. https://doi.org/10.1158/0008-5472.CAN-10-1666.
22. Le, A., Lane, A.N., Hamaker, M., Bose, S., Gouw, A., Barbi, J., Tsukamoto, T., Rojas, C.J., Slusher, B.S., Zhang, H., et al. (2012). Glucose-independent glutamine metabolism via TCA cycling for proliferation and survival in B cells. Cell Metab. *15*, 110–121. https://doi.org/10.1016/j.cmet.2011.12.009.
23. van den Heuvel, A.P.J., Jing, J., Wooster, R.F., and Bachman, K.E. (2012). Analysis of glutamine dependency in non-small cell lung cancer: GLS1 splice variant GAC is essential for cancer cell growth. Cancer Biol. Ther. *13*, 1185–1194. https://doi.org/10.4161/cbt.21348.
24. Gross, M.I., Demo, S.D., Dennison, J.B., Chen, L., Chernov-Rogan, T., Goyal, B., Janes, J.R., Laidig, G.J., Lewis, E.R., Li, J., et al. (2014). Antitumor activity of the glutaminase inhibitor CB-839 in triple-negative breast cancer. Mol. Cancer Ther. *13*, 890–901. https://doi.org/10.1158/1535-7163.MCT-13-0870.
25. Gregory, M.A., Nemkov, T., Park, H.J., Zaberezhnyy, V., Gehrke, S., Adane, B., Jordan, C.T., Hansen, K.C., D'Alessandro, A., and DeGregori, J. (2019). Targeting glutamine metabolism and redox state for leukemia therapy. Clin. Cancer Res. *25*, 4079–4090. https://doi.org/10.1158/1078-0432.CCR-18-3223.
26. Shah, R., Singh, S.J., Eddy, K., Filipp, F.V., and Chen, S. (2019). Concurrent targeting of glutaminolysis and metabotropic glutamate receptor 1 (GRM1) reduces glutamate bioavailability in GRM1(+) melanoma. Cancer Res. *79*, 1799–1809. https://doi.org/10.1158/0008-5472.CAN-18-1500.
27. Zeng, M., Kwiatkowski, N.P., Zhang, T., Nabet, B., Xu, M., Liang, Y., Quan, C., Wang, J., Hao, M., Palakurthi, S., et al. (2018). Targeting MYC dependency in ovarian cancer through inhibition of CDK7 and CDK12/13. eLife *7*. https://doi.org/10.7554/eLife.39030.
28. Reyes-González, J.M., Armaiz-Peña, G.N., Mangala, L.S., Valiyeva, F., Ivan, C., Pradeep, S., Echevarría-Vargas, I.M., Rivera-Reyes, A., Sood, A.K., and Vivas-Mejía, P.E. (2015). Targeting c-MYC in platinum-resistant ovarian cancer. Mol. Cancer Ther. *14*, 2260–2269. https://doi.org/10.1158/1535-7163.MCT-14-0801.
29. Thng, D.K.H., Toh, T.B., and Chow, E.K.H. (2021). Capitalizing on synthetic lethality of MYC to treat cancer in the digital age. Trends Pharmacol. Sci. *42*, 166–182. https://doi.org/10.1016/j.tips.2020.11.014.
30. Yang, D., Liu, H., Goga, A., Kim, S., Yuneva, M., and Bishop, J.M. (2010). Therapeutic potential of a synthetic lethal interaction between the MYC proto-oncogene and

inhibition of aurora-B kinase. Proc. Natl. Acad. Sci. USA *107*, 13836–13841. https://doi.org/10.1073/pnas.1008366107.

31. Mertz, J.A., Conery, A.R., Bryant, B.M., Sandy, P., Balasubramanian, S., Mele, D.A., Bergeron, L., and Sims, R.J., 3rd (2011). Targeting MYC dependence in cancer by inhibiting BET bromodomains. Proc. Natl. Acad. Sci. USA *108*, 16669–16674. https://doi.org/10.1073/pnas.1108190108.

32. Vomund, S., Schäfer, A., Parnham, M.J., Brüne, B., and von Knethen, A. (2017). Nrf2, the master regulator of anti-oxidative responses. Int. J. Mol. Sci. *18*, 2772. https://doi.org/10.3390/ijms18122772.

33. Sakurai, A., Nishimoto, M., Himeno, S., Imura, N., Tsujimoto, M., Kunimoto, M., and Hara, S. (2005). Transcriptional regulation of thioredoxin reductase 1 expression by cadmium in vascular endothelial cells: role of NF-E2-related factor-2. J. Cell. Physiol. *203*, 529–537. https://doi.org/10.1002/jcp.20246.

34. Roder, C., and Thomson, M.J. (2015). Auranofin: repurposing an old drug for a golden new age. Drugs R. D. *15*, 13–20. https://doi.org/10.1007/s40268-015-0083-y.

35. Leist, M., Raab, B., Maurer, S., Rösick, U., and Brigelius-Flohé, R. (1996). Conventional cell culture media do not adequately supply cells with antioxidants and thus facilitate peroxide-induced genotoxicity. Free Radic. Biol. Med. *21*, 297–306. https://doi.org/10.1016/0891-5849(96)00045-7.

36. Karlenius, T.C., Shah, F., Yu, W.C., Hawkes, H.J.K., Tinggi, U., Clarke, F.M., and Tonissen, K.F. (2011). The selenium content of cell culture serum influences redox-regulated gene expression. Biotechniques *50*, 295–301. https://doi.org/10.2144/000113666.

37. Sabatier, P., Beusch, C.M., Gencheva, R., Cheng, Q., Zubarev, R., and Arnér, E.S.J. (2021). Comprehensive chemical proteomics analyses reveal that the new TRi-1 and TRi-2 compounds are more specific thioredoxin reductase 1 inhibitors than auranofin. Redox Biol. *48*, 102184. https://doi.org/10.1016/j.redox.2021.102184.

38. Stafford, W.C., Peng, X., Olofsson, M.H., Zhang, X., Luci, D.K., Lu, L., Cheng, Q., Trésaugues, L., Dexheimer, T.S., Coussens, N.P., et al. (2018). Irreversible inhibition of cytosolic thioredoxin reductase 1 as a mechanistic basis for anticancer therapy. Sci. Transl. Med. *10*, eaaf7444. https://doi.org/10.1126/scitranslmed.aaf7444.

39. Raninga, P.V., Di Trapani, G., Vuckovic, S., and Tonissen, K.F. (2016). TrxR1 inhibition overcomes both hypoxia-induced and acquired bortezomib resistance in multiple myeloma through NF-small ka, Cyrillicbeta inhibition. Cell Cycle *15*, 559–572. https://doi.org/10.1080/15384101.2015.1136038.

40. Raninga, P.V., Trapani, G.D., and Tonissen, K.F. (2014). Cross talk between two antioxidant systems, thioredoxin and DJ-1: consequences for cancer. Oncoscience *1*, 95–110. https://doi.org/10.18632/oncoscience.12.

41. Saei, A.A., Gullberg, H., Sabatier, P., Beusch, C.M., Johansson, K., Lundgren, B., Arvidsson, P.I., Arnér, E.S.J., and Zubarev, R.A. (2020). Comprehensive chemical proteomics for target deconvolution of the redox active drug auranofin. Redox Biol. *32*, 101491. https://doi.org/10.1016/j.redox.2020.101491.

42. Go, Y.M., and Jones, D.P. (2013). The redox proteome. J. Biol. Chem. *288*, 26512–26520. https://doi.org/10.1074/jbc.R113.464131.

43. Sherman, B.T., Hao, M., Qiu, J., Jiao, X., Baseler, M.W., Lane, H.C., Imamichi, T., and Chang, W. (2022). DAVID: a web server for functional enrichment analysis and functional annotation of gene lists (2021 update). Nucleic Acids Res. *50*, W216–W221. https://doi.org/10.1093/nar/gkac194.

44. Huang, D.W., Sherman, B.T., and Lempicki, R.A. (2009). Systematic and integrative analysis of large gene lists using DAVID bioinformatics resources. Nat. Protoc. *4*, 44–57. https://doi.org/10.1038/nprot.2008.211.

45. Gao, P., Tchernyshyov, I., Chang, T.C., Lee, Y.S., Kita, K., Ochi, T., Zeller, K.I., De Marzo, A.M., Van Eyk, J.E., Mendell, J.T., and Dang, C.V. (2009). c-Myc suppression of miR-23a/b enhances mitochondrial glutaminase expression and glutamine metabolism. Nature *458*, 762–765. https://doi.org/10.1038/nature07823.

46. Bott, A.J., Peng, I.C., Fan, Y., Faubert, B., Zhao, L., Li, J., Neidler, S., Sun, Y., Jaber, N., Krokowski, D., et al. (2015). Oncogenic myc induces expression of glutamine synthetase through promoter demethylation. Cell Metab. *22*, 1068–1077. https://doi.org/10.1016/j.cmet.2015.09.025.

47. Yuneva, M.O., Fan, T.W.M., Allen, T.D., Higashi, R.M., Ferraris, D.V., Tsukamoto, T., Matés, J.M., Alonso, F.J., Wang, C., Seo, Y., et al. (2012). The metabolic profile of tumors depends on both the responsible genetic lesion and tissue type. Cell Metab. *15*, 157–170. https://doi.org/10.1016/j.cmet.2011.12.015.

48. Sappington, D.R., Siegel, E.R., Hiatt, G., Desai, A., Penney, R.B., Jamshidi-Parsian, A., Griffin, R.J., and Boysen, G. (2016). Glutamine drives glutathione synthesis and contributes to radiation sensitivity of A549 and H460 lung cancer cell lines. Biochim. Biophys. Acta *1860*, 836–843. https://doi.org/10.1016/j.bbagen.2016.01.021.

49. Sato, H., Tamba, M., Ishii, T., and Bannai, S. (1999). Cloning and expression of a plasma membrane cystine/glutamate exchange transporter composed of two distinct proteins. J. Biol. Chem. *274*, 11455–11458. https://doi.org/10.1074/jbc.274.17.11455.

50. Yang, P., Luo, X., Li, J., Zhang, T., Gao, X., Hua, J., Li, Y., Ding, N., He, J., Zhang, Y., et al. (2021). Ionizing radiation upregulates glutamine metabolism and induces cell death via accumulation of reactive oxygen species. Oxid. Med. Cell. Longev. *2021*, 5826932. https://doi.org/10.1155/2021/5826932.

51. Sze, J.H., Raninga, P.V., Nakamura, K., Casey, M., Khanna, K.K., Berners-Price, S.J., Di Trapani, G., and Tonissen, K.F. (2020). Anticancer activity of a Gold(I) phosphine thioredoxin reductase inhibitor in multiple myeloma. Redox Biol. *28*, 101310. https://doi.org/10.1016/j.redox.2019.101310.

52. Karsa, M., Kosciolek, A., Bongers, A., Mariana, A., Failes, T., Gifford, A.J., Kees, U.R., Cheung, L.C., Kotecha, R.S., Arndt, G.M., et al. (2021). Exploiting the reactive oxygen species imbalance in high-risk paediatric acute lymphoblastic leukaemia through auranofin. Br. J. Cancer *125*, 55–64. https://doi.org/10.1038/s41416-021-01332-x.

53. Su, Z., Burchfield, J.G., Yang, P., Humphrey, S.J., Yang, G., Francis, D., Yasmin, S., Shin, S.Y., Norris, D.M., Kearney, A.L., et al. (2019). Global redox proteome and phosphoproteome analysis reveals redox switch in Akt. Nat. Commun. *10*, 5486. https://doi.org/10.1038/s41467-019-13114-4.

54. Chiappetta, G., Gamberi, T., Faienza, F., Limaj, X., Rizza, S., Messori, L., Filomeni, G., Modesti, A., and Vinh, J. (2022). Redox proteome analysis of auranofin exposed ovarian cancer cells (A2780). Redox Biol. *52*, 102294. https://doi.org/10.1016/j.redox.2022.102294.

55. Barnes, B.M., Nelson, L., Tighe, A., Burghel, G.J., Lin, I.H., Desai, S., McGrail, J.C., Morgan, R.D., and Taylor, S.S. (2021). Distinct transcriptional programs stratify ovarian cancer cell lines into the five major histological subtypes. Genome Med. *13*, 140. https://doi.org/10.1186/s13073-021-00952-5.

56. Peralta, D., Bronowska, A.K., Morgan, B., Dóka, É., Van Laer, K., Nagy, P., Gräter, F., and Dick, T.P. (2015). A proton relay enhances H2O2 sensitivity of GAPDH to facilitate metabolic adaptation. Nat. Chem. Biol. *11*, 156–163. https://doi.org/10.1038/nchembio.1720.

57. Mandal, P.K., Schneider, M., Kölle, P., Kuhlencordt, P., Förster, H., Beck, H., Bornkamm, G.W., and Conrad, M. (2010). Loss of thioredoxin reductase 1 renders tumors highly susceptible to pharmacologic glutathione deprivation. Cancer Res. *70*, 9505–9514. https://doi.org/10.1158/0008-5472.CAN-10-1509.

58. Varghese, S., Pramanik, S., Williams, L.J., Hodges, H.R., Hudgens, C.W., Fischer, G.M., Luo, C.K., Knighton, B., Tan, L., Lorenzi, P.L., et al. (2021). The glutaminase inhibitor CB-839 (telaglenastat) enhances the antimelanoma activity of T-cell-mediated immunotherapies. Mol. Cancer Ther. *20*, 500–511. https://doi.org/10.1158/1535-7163.MCT-20-0430.

59. Jin, H., Wang, S., Zaal, E.A., Wang, C., Wu, H., Bosma, A., Jochems, F., Isima, N., Jin, G., Lieftink, C., et al. (2020). A powerful drug combination strategy targeting glutamine addiction for the treatment of human liver cancer. eLife *9*, e56749. https://doi.org/10.7554/eLife.56749.

60. Liu, J.F., Palakurthi, S., Zeng, Q., Zhou, S., Ivanova, E., Huang, W., Zervantonakis, I.K., Selfors, L.M., Shen, Y., Pritchard, C.C., et al. (2017). Establishment of patient-derived tumor xenograft models of epithelial ovarian cancer for preclinical evaluation of novel therapeutics. Clin. Cancer Res. *23*, 1263–1273. https://doi.org/10.1158/1078-0432.CCR-16-1237.

61. Robinson, M.D., McCarthy, D.J., and Smyth, G.K. (2010). edgeR: a Bioconductor package for differential expression analysis of digital gene expression data. Bioinformatics *26*, 139–140. https://doi.org/10.1093/bioinformatics/btp616.

62. Subramanian, A., Tamayo, P., Mootha, V.K., Mukherjee, S., Ebert, B.L., Gillette, M.A., Paulovich, A., Pomeroy, S.L., Golub, T.R., Lander, E.S., and Mesirov, J.P. (2005). Gene set enrichment analysis: a knowledge-based approach for interpreting genome-wide expression profiles. Proc. Natl. Acad. Sci. USA *102*, 15545–15550. https://doi.org/10.1073/pnas.0506580102.

63. Mootha, V.K., Lindgren, C.M., Eriksson, K.F., Subramanian, A., Sihag, S., Lehar, J., Puigserver, P., Carlsson, E., Ridderstråle, M., Laurila, E., et al. (2003). PGC-1alpha-responsive genes

involved in oxidative phosphorylation are coordinately downregulated in human diabetes. Nat. Genet. *34*, 267–273. https://doi.org/10.1038/ng1180.

64. Liberzon, A., Birger, C., Thorvaldsdóttir, H., Ghandi, M., Mesirov, J.P., and Tamayo, P. (2015). The Molecular Signatures Database (MSigDB) hallmark gene set collection. Cell Syst. *1*, 417–425. https://doi.org/10.1016/j.cels.2015.12.004.

65. Tiwari, R., Sahu, I., Soni, B.L., Sathe, G.J., Datta, K.K., Thapa, P., Sinha, S., Vadivel, C.K., Dhaka, B., Gowda, H., et al. (2017). Quantitative phosphoproteomic analysis reveals system-wide signaling pathways regulated by site-specific phosphorylation of Keratin-8 in skin squamous cell carcinoma derived cell line. Proteomics *17*, 1600254.

66. Espinosa, M.I., Gonzalez-Garcia, R.A., Valgepea, K., Plan, M.R., Scott, C., Pretorius, I.S., Marcellin, E., Paulsen, I.T., and Williams, T.C. (2020). Adaptive laboratory evolution of native methanol assimilation in Saccharomyces cerevisiae. Nat. Commun. *11*, 5564. https://doi.org/10.1038/s41467-020-19390-9.